RSC Advances

ROYAL SOCIETY OF CHEMISTRY

www.rsc.org/advances

Journal Name

ARTICLE

Controllable Synthesis of Graphene Using Novel Aromatic 1,3,5-Triethynylbenzene Molecules on Rh(111)

Received 00th January 20xx,
Accepted 00th January 20xx

DOI: 10.1039/x0xx00000x

www.rsc.org/

Yue Qi,[a] Xiebo Zhou,[b] Mengxi Liu,[a] Qiucheng Li,[a] Donglin Ma,[a] Yanfeng Zhang,[a,b]* and Zhongfan Liu[a]*

Selecting distinctive carbon precursors can mediate graphene synthesis towards versatile targets, for example, using C_{60} to produce graphene quantum dots or hexabromobenzene to achieve graphene at rather low temperature. Herein, 1,3,5-triethynylbenzene (TEB) is selected for the first time as the carbon precursor for graphene synthesis on Rh(111). Considering of the characteristic π-d orbital hybridization between TEB and Rh(111), room-temperature adsorption followed with a temperature-programmed annealing or direct annealing to target growth temperature under the ultrahigh vacuum conditions are designed to be the two synthesis pathways. In the former growth pathway, the benzene ring of the TEB unit is expected to be maintained throughout the whole annealing process, leading to high yielding graphene at relatively low temperature as compared with existing synthesis *via* gaseous precursors. Several-molecule oligomers and graphene nanoclusters are detected to be the crucial intermediates through ste-pwise annealing (150 °C and 430 °C), as evidenced by scanning tunneling microscopy (STM) characterizations. Interestingly, graphene synthesized *via* the latter pathway usually possesses less domain boundaries and defects than the former one, probably due to sufficient diffusion and rearrangement of carbon precursors. Briefly, this work should contribute greatly to understanding the growth intermediates and the synthesis of high-quality graphene using large aromatic precursor molecules.

Introduction

Graphene has recently attracted considerable attentions because of its exceptional electronic, thermal, optical properties and related applications in high-frequency transistor, transparent electrode, touch screen, photodetector,[1-6] *etc*. In order to fulfil its potentials, diverse approaches have been developed for achieving high-quality, thickness controllable graphene samples, such as, mechanical exfoliation from highly oriented pyrolytic graphite (HOPG),[1] epitaxial growth on silicon carbide (SiC)[7-10] and reduction of graphene oxide (GO),[11] *etc*.

In particular, chemical vapor deposition (CVD) has shown great promise in synthesizing graphene films with large area, large domain size and uniform thickness on copper and nickel substrates.[2, 10, 12-15] Specifically, ultrahigh vacuum CVD (UHV-CVD) method was also exploited and combined with an atomically-resolved characterization method of scanning tunneling microscopy (STM). This allows for an *in-situ* imaging of the atomic structure, grain boundary, defect, stacking order, *etc*. More significantly, this combination also facilitates a deep understanding of the dynamic growth process *via* an *in-situ* imaging of the growth intermediates under different growth temperature,[16, 17] which, in turn, sheds some light on the graphene synthesis using traditional CVD methods.

In the UHV system, single crystalline transition metals, such as Ru(0001),[18, 19] Ni(111),[20, 21] Pt(111),[22] Pd(111),[23] Ir(111),[24-26] Cu(111),[13] Ag(111),[14] Rh(111),[27] were more preferentially used for graphene synthesis due to their flatter surfaces and more explicit crystallographic planes than that of metal foils used in traditional CVD synthesis.[28] Gaseous carbon precursors, *e.g.,* methane[2, 10, 12] and ethylene[19, 25, 29-32] have been widely used for graphene synthesis, due to their low cost, wide availability and ease of operation. Interestingly, many aromatic derivatives have also exhibited great potential in synthesizing distinctive graphene structures, (hexabenzocoronene (HBC) and coronene on Co (0001)[33] and Ru(0001),[34] respectively), for exploring the novel electronic properties of graphene nanoislands or synthesizing graphene nanoclusters. Additionally, polyphenylene and C_{60} have also been used for easily processable, chemically tailored nanographenes on Cu(111)[35] and geometrically well-defined graphene quantum dots on Ru(0001),[16] respectively.

Moreover, in the graphene synthesis, disparate molecule-substrate, molecule-molecule interactions and different annealing modes usually result in distinct graphene growth behaviours in UHV. This is probably mediated by the disparate surface actions of deposited precursor molecules, such as adsorption, catalytic decomposition, diffusion and subsequent

[a] Center for Nanochemistry, Beijing Science and Engineering Center for Nanocarbons, Beijing National Laboratory for Molecular Sciences, College of Chemistry and Molecular Engineering, Academy for Advanced Interdisciplinary Studies, Peking University, Beijing 100871, China
[b] Department of Materials Science and Engineering, College of Engineering, Peking University, Beijing 100871, China
E-mail: zfliu@pku.edu.cn，yanfengzhang@pku.edu.cn
† Electronic Supplementary Information (ESI) available: [details of any supplementary information available should be included here]. See DOI: 10.1039/x0xx00000x

nucleation on the metal surface. In this regard, for the graphene synthesis using aromatic derivatives, comparative investigations of the graphene synthesis under different annealing growth pathways are highly desired.

In this work, we select 1,3,5-triethynylbenzene (TEB) (Fig. 1a), which possesses a distinctive π-conjugated system including a novel CH≡C moiety as the carbon precursor. Rh(111) is selected as the growth substrate since it may afford strong molecule-substrate interaction *via* the characteristic π-d orbital hybridization even at room temperature (RT). This largely reduces the desorption of TEB intermediates during graphene synthesis *via* high temperature annealing, hereby leading to high-yield production. Two annealing pathways were designed for graphene synthesis after room temperature adsorption, *i.e.* temperature-programmed annealing or direct annealing to target growth temperature. This is suitable for exploring the effects of different annealing modes on the structural evolutions of precursor molecules during graphene synthesis. Furthermore, comparison studies on the crystal quality and growth mechanisms of graphene obtained from the two pathways are probed with the aid of STM characterization.

Results and Discussion

TEB (Fig. 1a) is a member of aromatic hydrocarbons that contains both sp^2-hybridized benzene ring and *sp*-hybridized CH≡C moiety forming a π-conjugated system. This π-conjugated feature may facilitate its adsorption and assembly on some single crystal substrates.[36, 37] In order to realize the steady thermal evaporation of TEB, an insight into the thermal stability and pyrolysis of the TEB molecule was highly needed under different heating temperature. Thermogravimetry-Mass (TG-MS)[38-40] experiments were thus performed with the results shown in Fig. 1b and Fig. S1 †, respectively.

It can be noticed that the reduction of the relative mass begins at ~130 °C and then terminates at ~150 °C, along with a weight loss percentage up to 88% (Fig. 1b). This observation indicates that most of the molecules can be sublimated at ~150 °C, which makes TEB suitable for graphene synthesis. Meanwhile, in the MS curve, the ion current becomes detectable at ~150 °C, highly suggestive of the presence of pyrolysis fragments of TEB. The assessments of these fragments are marked in the MS curve in Fig. S1. † Peak 1 (m/z=150) represents $C_{12}H_6$ which is assigned to the volatilization of the intact TEB. Moreover, some other peaks can also be recognized with their assessments described in Fig. S1. † Rh(111) was selected as the substrate for graphene synthesis, considering of its strong interaction with TEB *via* the characteristic π-d orbital hybridization.[27, 32, 37, 41, 42]

During the experiments, TEB molecules were sublimated at ~107 °C, [43, 44] and deposited onto Rh(111) held at room temperature (RT) under ultrahigh vacuum (UHV) conditions. The morphology of TEB molecules adsorbed on Rh(111) was characterized at a nominal coverage of 0.1 monolayer (ML) (Fig. 1c). Bright individual spot-like contrasts possessing a uniform diameter of ~9.00 Å and an apparent height of ~0.36 Å were commonly observed, consistent with the theoretical

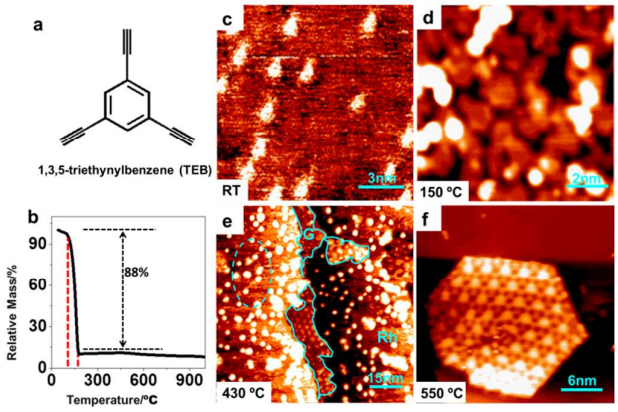

Fig. 1. (a) Structure of a 1,3,5-triethynylbenzene (TEB) molecule. (b) Thermogravimetry (TG) curve of TEB. In TG spectrum, weight loss percentage approaches 88% from room temperature to 150 °C. (c-f) Corresponding STM images for TEB molecules evaporated at ~107 °C with Rh(111) hold at RT, and after annealed at 150 °C, 430 °C and 550 °C, respectively. (Scanning conditions: (c) V_T = − 0.03 V, I_T = 0.93 nA; (d) − 0.86 V, 0.60 nA; (e) − 0.37 V, 2.13 nA; (f) − 0.37 V, 2.13 nA.)

value of the flat-lying TEB molecule.[37, 45] When TEB molecules with larger coverage (~0.6 ML) than that in Fig. 1c (~0.1ML) were deposited onto Rh(111) at room temperature (RT), dimeric products with a lateral size of ~2 nm along the long axis direction can be resolved as shown in Fig. S2. † Based on the different STM images of the samples possessing lower and higher coverage (Fig. 1c and Fig. S2, † respectively), it can be concluded that the morphology of TEB on the metal substrate is coverage dependent.

Intriguingly, after thermal annealing a nominal 1.2 ML TEB on Rh(111) at 150 °C for 10 minutes, several-molecule oligomers come into being, which can spread over the surface to form a near full layer. Additional oligomers adsorbed on top are also observable by STM due to their higher contrasts than the under layer (Fig. 1d). By annealing as-deposited sub-monolayer TEB molecules at 430 °C for 10 min, uniform nanoclusters and islands can be evolved. The nanoclusters tend to distribute uniformly on the terraces of Rh(111), while the islands preferentially evolve along the substrate step edges (Fig. 1e). This growth feature can be attributed to the rather high attaching probability of nanoclusters at the step edges. In the islands, moiré pattern which is typical for graphene on Rh(111) can be recognized with a fixed period of ~2.88 nm.[27] This possibly implies that graphene starts to form at the temperature of 430 °C. Compared with the small gaseous precursors (such as methane and ethylene usually forming graphene nanoclusters at ~600 °C on Rh(111) or Ru(0001)),[19, 34, 46] aromatic TEB precursor presents relatively low growth temperature for synthesis of graphene nanoclusters. This could be explained by the fact that the benzene rings of the TEB molecules are largely maintained and act as the

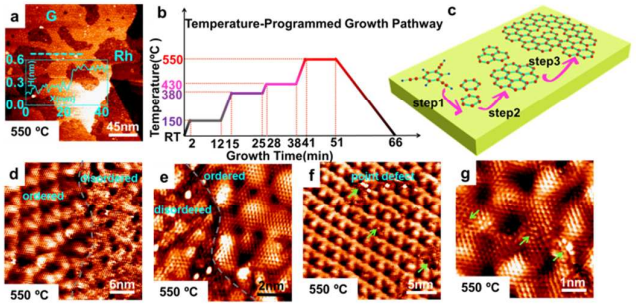

Fig. 2. STM images of graphene synthesized through annealing as-deposited TEB molecules with a temperature-programmed annealing growth pathway. (a) Large scale STM image of the finally obtained graphene. For graphene regions, the section-view along the dashed line presents a uniform height of ~0.27 nm. (b, c) Schematic diagrams of the temperature-programmed annealing growth pathway. (d, e) Sequential zoom-in STM images on the boundaries of ordered and disordered graphene regions. (f) Point defects observed inside the ordered moiré superstructure (marked by green arrows). (g) Further zoom-in STM image around the point defects. (Scanning conditions: (a) V_T = – 0.08 V, I_T = 2.84 nA; (d) – 0.01 V, 16.30 nA; (e) – 0.01 V, 7.85 nA; (f) – 0.02 V, 5.36 nA; (g) – 0.02 V, 12.64 nA.)

fundamental building blocks for graphene growth. After further annealing treatment of the same sample at 550 °C for 10 min, perfect hexagonal graphene islands can be synthesized, as evidenced by the uniform long range moiré superstructures (Fig. 1f). With these results, it can be inferred that, high-quality graphene can be synthesized on Rh(111) *via* step-wise annealing of the room temperature adsorbed TEB precursors. For more details, the STM images of other intermediates evolving at different annealing temperature are displayed in Fig. S3. †

In the growth of graphene by using TEB precursors, it is intriguing to find that the quality of graphene varies significantly with different growth pathways. A temperature-programmed annealing growth pathway, *i.e.* step-wise annealing at 150 °C, 380 °C, 430 °C and then 550 °C (Fig. 2b) was firstly performed on as-deposited monolayer TEB precursors. The STM characterizations were then performed on the sample after the whole step-wise annealing growth pathway, as shown in Fig. 2a.The brighter regions should be ascribed to graphene areas, and the darker regions are attributed to the bare Rh(111). For graphene covered regions, an apparent height of ~0.27 nm can be deduced from the height profile in Fig. 2a, well consistent with the reported data for graphene synthesis on Rh(111) synthesized with C_2H_4 precursors.[32]

The homo-coupling reaction of terminal alkynes among TEB molecules have been reported by Y. Q. Zhang *et al.*[36] In their work, with the purpose to achieve TEB dimeric products, the initial annealing temperature was set at as low as ~300 K. In contrast, the purpose of this work is to synthesize graphene with TEB precursors, and a step-wise annealing process is thus utilized to realize this purpose. The initial annealing temperature was set at above 150°C, which is much higher than that of annealing TEB on Ag(111) for evolving coupling structures. To illustrate the possible reactions under the current pathway, a schematic view is plotted in Fig. 2c. Through annealing at ~150 °C, the CH≡C units of TEB may be removed from the C_6H_3 unit (step 1, the C_6H_3 unit is possibly dehydrogenated). At even higher temperature from 380 °C to 430 °C, the C_6H_3 units are totally dehydrogenated into benzene rings, which then bind with each other to form large-scale graphene step by step (step 2 and 3). In this growth pathway, the benzene rings of the TEB molecules are largely maintained and act as the fundamental building blocks for graphene growth. This may explain why the synthesis temperature involved in this method is rather low (430 °C) as compared with those using gaseous precursors (methane, ethylene, propene *etc.*) at about 700-1000 °C on the same substrate of Rh(111).[27, 41, 47-51] Similarly, the low-temperature (220 °C) synthesis of graphene was also reported by L. Jiang *et al. via* a radical-coupling reaction by the effectively breaking of the C–Br bonds of hexabromobenzene.[52]Further detailed STM observations reveal that the graphene synthesized with this pathway usually shows the coexistence of ordered and disordered graphene moiré regions (Fig. 2d, after 550 °C annealing). In the ordered areas, long range graphene moiré can be identified with a period of ~2.88 nm (Fig. 2e), evolving from 12 × 12 C-C on 11 × 11 Rh(111) according to the published references.[27, 32] The evolution of ordered large-area graphene moiré usually suggests the formation of large-area uniform monolayer graphene. However, in the disordered regions, no continuous graphene moiré can be observed. Instead, high density defects occur frequently inside the graphene lattices.

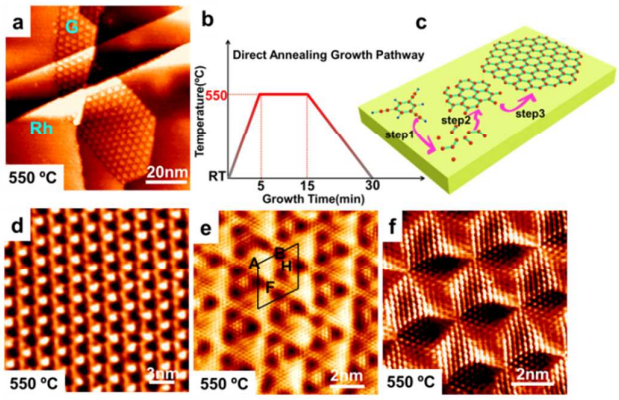

Fig. 3. STM images of graphene synthesized by direct annealing as-deposited TEB molecules at 550 °C for 10 min. (a) STM image of graphene evolved along the step edges of Rh(111). (b, c) Schematic diagrams of the direct annealing growth pathway and the related surface reactions. (d) Perfect moiré superstructures with a fixed period of ~2.88 nm. (e, f) Atomic resolution STM images of the obtained graphene. The ATOP

(A), HCP (H), FCC (F), BRIDGE (B) regions are marked in (e), respectively. (Scanning conditions: (a) V_T = − 0.46 V, I_T = 0.80 nA; (d) − 0.01 V, 2.35 nA; (e) − 0.03 V, 0.20 nA; (f) − 0.01 V, 17.93 nA.)

Moreover, inside the relatively uniform graphene moiré (Fig. 2f, g), some point defects can also be discerned (marked with green arrows) causing local graphene lattices broken. Notably, these point defects can also induce the increase of the local density of states in graphene and lead to different STM contrasts.[53-55] To explain the origin of the defects, with this growth pathway, oligomers evolved at relatively low temperature (150 °C), and their relatively high mass and coverage (corresponding to limited space) may hinder the surface diffusion and the subsequent patching growth of graphene.

In order to clarify the effects of different annealing modes on the synthesis of graphene and to improve the quality of graphene, a new growth pathway was also designed by annealing as-deposited TEB precursors on Rh(111) directly (in 5 min) to 550 °C and then keeping on annealing for 10 min, as schematically shown in Fig. 3b. Ordered graphene islands are observed to preferentially reside along the step edges of Rh(111) (Fig. 3a). Note that, with this growth pathway, a monolayer TEB adsorption at room temperature usually brings about nominal graphene coverage of ~30% which is much lower than that of the former growth pathway (~80%). In the direct annealing process, the TEB precursors are considered to dissociate instantly into carbon fragments (Fig. 3c, step 1), which diffuse on the surface and coalesce with each other (Fig. 3c, step 2), with the formation of large graphene islands (Fig. 3c, step 3).

Further zoom-in STM image of the graphene area presents perfect moiré superstructures with a fixed period of ~2.88 nm (Fig. 3d).[27, 32] And atomic scale STM images (Fig. 3e,f) over such area usually present perfect atomic lattices and periodic graphene moirés, suggestive of the formation of high quality graphene. Notably, under different tunneling or tip conditions, the graphene moirés exhibit different STM contrasts (Fig. 3d, e and f), which are mainly attributed to the various C-Rh registries at different locations inside per supercell.[27, 32, 41, 56] The location marked by the black capital letter A showing bright contrast in the supercell corresponds to carbon atoms standing over Rh atoms in the second and third layers (or ATOP). Here, the graphene lattice in such a region is most weakly bounded to the Rh substrate. The locations F and H, presenting relatively bright contrasts on the long diagonal of the rhombus, should be in line with FCC (carbon atoms placed above Rh atoms in the first and second layers) and HCP (carbon atoms placed above Rh atoms in the first and third layers), respectively. The location B (called as BRIDGE, Rh atoms in the first layer bridging the carbon atoms) demonstrate the darkest contrast, indicative of the strongest interaction between graphene and Rh(111). In general, according to abundant STM observations of various samples, it can be concluded that, the crystal quality of graphene synthesized with the current growth pathway seems superior to that with the temperature-programmed growth pathway. SEM image of graphene synthesized by the direct annealing growth pathway with coverage at ~70% is shown in Fig. S5a. † Note that, the Raman signal of graphene on Rh is usually suppressed by the substrate effect, hereby the typical bands of graphene (2D band at ~2680 cm^{-1} to G band at ~1584 cm^{-1}) are absent as shown in Fig. S5b. † In order to show the crystal quality of graphene synthesized through temperature-programmed and direct annealing growth pathways, amounts of large-scale STM images were then captured for the two kind samples, with the typical results shown in Fig. S4. † Obviously, the latter sample possesses higher crystal quality than that of the former one. An intriguing phenomenon observed in this growth pathway is that, by annealing as-deposited sub-monolayer TEB molecules at 430 °C for 10 min, mono-dispersed nanoclusters and nanoislands were imaged with bright spots and large-period superstructures, respectively (Fig. 4a).

The nanoclusters can be classified into two groups with different diameters (~1.00 nm and ~1.60 nm) according to the line profiles in Fig. 4d, e. Very recently, similar nanoclusters have been observed for graphene growth on Ir(111),[24] Ru(0001),[19, 34] Rh(111),[46] and Cu(110).[57] They reported that the most possible structure of the relatively smaller nanoclusters (~1.00 nm in diameter) was C_{24} which should resemble that of a fully dehydrogenated coronene. The structure of the larger nanoclusters (~1.60 nm in diameter) should be C_{24} carbon skeletons surrounded by protons.

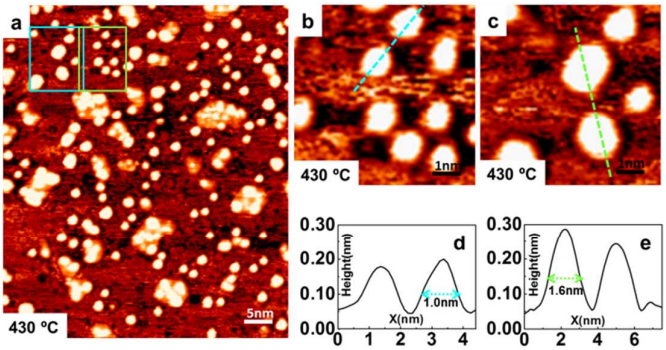

Fig. 4. STM images of coexisting graphene nanoclusters and islands evolved from annealing sub-monolayer TEB molecules at 430 °C for 10 min. (a) Large-scale STM image of the surface. (b, c) Magnified STM images of small and large individual nanoclusters obtained from squares in (a), (blue and green squares corresponding to (b) and (c), respectively). (d, e) Line profiles taken along the dashed lines in (b, c) showing two kinds of individual nanoclusters with diameters of ~1.00 nm and ~1.60 nm, respectively. (Scanning conditions: (a) V_T = − 0.37 V, I_T = 2.13 nA; (b) − 0.37 V, 2.13 nA; (c) − 0.37 V, 2.13 nA.)

Experimental Section

Growth of Graphene on Rh(111): Sample preparations were performed in an ultrahigh vacuum system (base pressure, 1 × 10^{-10} mbar). The Rh(111) substrate (with purity of 99.999%) was processed by repetitive Ar^+ sputtering [p(Ar) = 5×10^{-6} mbar, I (ion current) = 12.0 μA] followed with post-annealing at 900K. TEB molecules (Sigma-Aldrich, nominal purity = 97%) were deposited on Rh(111) by heating a TEB-filled crucible of a Knudsen cell at 107 °C. The substrate was held at room temperature (RT) during the molecule deposition, and the deposition rate was controlled around 0.3 Å min^{-1}. The TEB molecules adsorbed on Rh(111) were then annealed in-situ to the target temperature.

For the step-wise annealing growth mode, the sample was not cooled down to room temperature to perform STM characterizations in the midway of the annealing process. That is to say, the STM characterizations were only performed after the whole annealing treatment. To get the intermediates at the intermediate annealing temperature, the sample was annealed to the target temperature and then cooled down to room temperature to perform STM characterizations. Characterization: The TG-MS experiments were performed simultaneously using a thermogravimeter (STA 449, Netzsch Instruments, Inc.) and a mass spectrometer (QMS 403C, Aëolos Instruments, Inc.). A constant temperature heating (150 °C) capillary was equipped between these two instruments to lead the formed gases from the TG furnace to the ion source. About 2-8 mg TEB molecules were decomposed with TG, and the gas products were introduced to the mass spectrometry for obtaining evolution curves. The sensitivity of the thermogravimeter used in this experiment was 0.001 mg. The STM examinations were performed by an Omicron UHV variable temperature STM, having a base pressure better than 10^{-10} mbar. The UHV-CVD sample was directly transferred from the preparation chamber into the STM chamber inside the vacuum system. All of the STM data was captured under a constant current mode with the sample hold at room-temperature.

Conclusions

In summary, we have performed the controlled synthesis of graphene *via* temperature-programmed annealing and direct annealing of room temperature deposited TEB precursors on Rh(111). High quality graphene has been obtained using direct annealing growth pathway. However, regarding the graphene synthesis *via* step-wise annealing pathway, the initial nucleation and subsequent growth of graphene can be achieved at relatively low temperature, as compared to those using gaseous precursors. In this regard, this work should shed light on the growth of high quality graphene with large aromatic molecules as precursors. Furthermore, inspired by the synthesis of pristine graphene using TEB molecules containing only C, H elements, this work should also be referential for synthesizing high-quality doped graphene using molecules containing other elements, such as B, N and S.

Acknowledgements

This work was financially supported by the National Natural Science Foundation of China (Grants 51222201, 51290272, 51472008, 51432002), the Ministry of Science and Technology of China (Grants 2012CB921404, 2013CB932603, 2012CB933404, 2011CB921903), and the Foundation for Innovative Research Groups of the National Natural Science Foundation of China (Grant 51121091).

Notes and references

1 K. S. Novoselov, A. K. Geim, S. V. Morozov, D. Jiang, Y. Zhang, S. V. Dubonos, I. V. Grigorieva and A. A. Firsov, *Science,* 2004, **306**, 666.
2 K. S. Kim, Y. Zhao, H. Jang, S. Y. Lee, J. M. Kim, K. S. Kim, J. H. Ahn, P. Kim, J. Y. Choi and B. H. Hong, *Nature,* 2009, **457**, 706.
3 S. Bae, H. Kim, Y. Lee, X. Xu, J. S. Park, Y. Zheng, J. Balakrishnan, T. Lei, H. R. Kim, Y. I. Song, Y. J. Kim, K. S. Kim, B. Ozyilmaz, J. H. Ahn, B. H. Hong and S. Iijima, *Nat. Nanotechnol.,* 2010, **5**, 574.
4 F. Bonaccorso, Z. Sun, T. Hasan and A. C. Ferrari, *Nature Photon.,* 2010, **4**, 611.
5 A. A. Balandin, *Nature Mater.,* 2011, **10**, 569.
6 K. S. Novoselov, V. I. Fal'ko, L. Colombo, P. R. Gellert, M. G. Schwab and K. Kim, *Nature,* 2012, **490**, 192.
7 C. Berger, Z. Song, X. Li, X. Wu, N. Brown, C. Naud, D. Mayou, T. Li, J. Hass, A. N. Marchenkov, E. H. Conrad, P. N. First and W. A. de Heer, *Science,* 2006, **312**, 1191.
8 T. Ohta, F. El Gabaly, A. Bostwick, J. L. McChesney, K. V. Emtsev, A. K. Schmid, T. Seyller, K. Horn and E. Rotenberg, *New J. Phys.,* 2008, **10**, 023034.
9 E. Rotenberg, A. Bostwick, T. Ohta, J. L. McChesney, T. Seyller and K. Horn, *Nature Mater.,* 2008, **7**, 258.
10 X. S. Li, W. W. Cai, A. Jinho, K. Seyoung, N. Junghyo, D. X. Yang, R. Piner, A. Velamakanni, J. Inhwa, E. Tutuc, S. K. Banerjee, L. Colombo and R. S. Ruoff, *Science,* 2009, **324**, 1312.
11 G. Eda, G. Fanchini and M. Chhowalla, *Nat. Nanotechnol.,* 2008, **3**, 270.
12 A. Reina, X. Jia, J. Ho, D. Nezich, H. Son, V. Bulovic, M. S. Dresselhaus and J. Kong, *Nano Lett.,* 2009, **9**, 30.
13 L. Gao, J. R. Guest, N. P. Guisinger, Nano Lett. 2010, **10**, 3512.
14 L. Gao, W. Ren, H. Xu, L. Jin, Z. Wang, T. Ma, L. P. Ma, Z. Zhang, Q. Fu, L.-M. Peng, X. Bao and H. M. Cheng, *Nat. Commun.,* 2012, **3**, 699.
15 S. Choubak, M. Biron, P. L. Levesque, R. Martel and P. Desjardins, *J. Phys. Chem. Lett.,* 2013, **4**, 1100.
16 J. Lu, P. S. E. Yeo, C. K. Gan, P. Wu and K. P. Loh, *Nat. Nanotechnol.,* 2011, **6**, 247.
17 B. Kiraly, E. V. Iski, A. J. Mannix, B. L. Fisher, M. C. Hersam and N. P. Guisinger, *Nat. Commun.,* 2013, **4**,2804.
18 P. W. Sutter, J. I. Flege and E. A. Sutter, *Nat. Mater.,* 2008, **7**, 406.
19 H. Zhang, Q. Fu, Y. Cui, D. Tan and X. H. Bao, *J. Phys. Chem. C*, 2009, **113**, 8296.
20 Y. S. Dedkov, M. Fonin, U. Ruediger and C. Laubschat, *Phys. Rev. Lett.,* 2008, **100**, 107602.
21 M. Olle, G. Ceballos, D. Serrate and P. Gambardella, *Nano Lett.,* 2012, **12**, 4431.
22 P. Sutter, J. T. Sadowski and E. Sutter, *Phys. Rev. B,* 2009, **80**, 245411.
23 S. Y. Kwon, C. V. Ciobanu, V. Petrova, V. B. Shenoy, J. Bareno, V. Gambin, I. Petrov and S. Kodambaka, *Nano Lett.* 2009, **9**, 3985.

24 J. Coraux, A. T. N'Diaye, M. Engler, C. Busse, D. Wall, N. Buckanie, F. j. M. Z. Heringdorf, R. van Gastel, B. Poelsema and T. Michely, *New J. Phys.,* 2009, **11**, 023006.
25 M. X. Liu, Y.C. Li, P. C. Chen, J. Y. Sun, D. L. Ma, Q. C. Li, T. Gao, Y. B. Gao, Z. H. Cheng, X. H. Qiu, Y. Fang, Y. F. Zhang and Z. F. Liu, *Nano Lett.,* 2014, **14**, 6342.
26 P. C. Rogge, S. Nie, K. F. McCarty, N. C. Bartelt and O. D. Dubon, *Nano Lett.,* 2014, **15**,170.
27 M. X. Liu, Y. B. Gao, Y. F. Zhang, Y. Zhang, D. L. Ma, Q. Q. Ji, T. Gao, Y. B. Chen and Z. F. Liu, *Small,* 2013, **9**, 1360.
28 R. He, L. Zhao, N. Petrone, K. S. Kim, M. Roth, J. Hone, P. Kim, A. Pasupathy and A. Pinczuk, *Nano Lett.,* 2012, **12**, 2408.
29 A. L. Vazquez de Parga, F. Calleja, B. Borca, M. C. G. Passeggi, Jr., J. J. Hinarejos, F. Guinea and R. Miranda, *Phys. Rev. Lett.,* 2008, **100**, 056807.
30 J. Coraux, A. T. N'Diaye, C. Busse and T. Michely, *Nano Lett.,* 2008, **8**, 565.
31 J. Lahiri, T. Miller, L. Adamska, I. I. Oleynik and M. Batzill, *Nano Lett.,* 2011, **11**, 518.
32 Y. B. Gao, Y. Zhang, P. C. Chen, Y. C. Li, M. X. Liu, T. Gao, D. L. Ma, Y. B. Chen, Z. H. Cheng, X. H. Qju, W. H. Duan and Z. F. Liu, *Nano Lett.,* 2013, **13**, 3439.
33 D. Eom, D. Prezzi, K. T. Rim, H. Zhou, M. Lefenfeld, S. Xiao, C. Nuckolls, M. S. Hybertsen, T. F. Heinz and G. W. Flynn, *Nano Lett.,* 2009, **9**, 2844.
34 Y. Cui, Q. Fu, H. Zhang and X. H. Bao, *Chem. Commun.,* 2011, **47**, 1470.
35 M. Treier, C. A. Pignedoli, T. Laino, R. Rieger, K. Muellen, D. Passerone and R. Fasel, *Nature Chem.,* 2011, **3**, 61.
36 Y. Q. Zhang, N. Kepčija, M. Kleinschrodt, K. Diller, S. Fischer, A. C. Papageorgiou, F. Allegretti, J. Björk, S. Klyatskaya, F. Klappenberger, M. Ruben and J. V. Barth, *Nat Commun.,* 2012, **3**, 1286.
37 N. Kepcija, Y. Q. Zhang, M. Kleinschrodt, J. Bjork, S. Klyatskaya, F. Klappenberger, M. Ruben and J. V. Barth, *J. Phys. Chem. C,* 2013, **117**, 3987.
38 G. Varhegyi, P. Szabo, F. Till, B. Zelei, M. J. Antal and X. F. Dai, *Energy Fuels,* 1998, **12**, 969.
39 Y. C. Chien, P. H. Shih and I. H. Hsien, *Environ. Eng. Sci.,* 2005, **22**, 601.
40 Y. C. Chien, M. Lu, M. Chai and F. J. Boreo, *Energy Fuels,* 2009, **23**, 202.
41 B. Wang, M. Caffio, C. Bromley, H. Früchtl and R. Schaub, *ACS Nano,* 2010, **4**, 5773.
42 D. Stradi, S. Barja, C. Diaz, M. Garnica, B. Borca, J. J. Hinarejos, D. Sanchez-Portal, M. Alcami, A. Arnau, A. L. Vazquez de Parga, R. Miranda and F. Martin, *Phys. Rev. Lett.,* 2011, **106**, 186102.
43 A. R. Campanelli, A. Arcadi, A. Domenicano, F. Ramondo and I. Hargittai, *J. Phys. Chem. A,* 2006, **110**, 2045.
44 J. Li, P. Huang, Beilstein, *J. Org. Chem.,* 2011, **7**, 426.
45 S. L. Yau, Y. G. Kim and K. Itaya, *J. Am. Chem. Soc.,* 1996, **118**, 7795.
46 B. Wang, X. F. Ma, M. Caffio, R. Schaub and W. X. Li, *Nano Lett.,* 2011, **11**, 424.
47 M. Sicot, S. Bouvron, O. Zander, U. Ruediger, Y. S. Dedkov and M. Fonin, *Appl. Phys. Lett.,* 2010, **96**, 093115.
48 M. Sicot, P. Leicht, A. Zusan, S. Bouvron, O. Zander, M. Weser, Y. S. Dedkov, K. Horn and M. Fonin, *ACS Nano,* 2012, **6**, 151.
49 G. C. Dong and J. W. M. Frenken, *ACS Nano,* 2013, **7**, 7028.
50 K. Gotterbarm, W. Zhao, O. Hofert, C. Gleichweit, C. Papp and H. P. Steinruck, *Phys. Chem. Chem. Phys.,* 2013, **15**, 19625.
51 Y. Zhang, Y. F. Zhang, D. L. Ma, Q. Q. Ji, W. Fang, J. P. Shi, T. Gao, M. X. Liu,Y. B. Gao, Y. B. Chen, L. M. Xu and Z. F. Liu, *Nano Res.,* 2013, **6**, 887.
52 L. Jiang, T. C. Niu, X. Q. Lu, H. L. Dong, W. Chen, Y. Q. Liu, W. P. Hu, and D. B. Zhu *J. Am. Chem. Soc.* 2013, **135**, 9050,
53 V. M. Pereira, F. Guinea, J. dos Santos, N. M. R. Peres and A. H. Castro Neto, *Phys. Rev. Lett.,* 2006, **96**, 036801.
54 G. M. Rutter, J. N. Crain, N. P. Guisinger, T. Li, P. N. First and J. A. Stroscio, *Science,* 2007, **317**, 219.
55 T. O. Wehling, A. Balatsky, M. Katsnelson, A. Lichtenstein, K. Scharnberg and R. Wiesendanger, *Phys. Rev. B,* 2007, **75**, 125425.
56 E. N. Voloshina, Y. S. Dedkov, S. Torbruegge, A. Thissen and M. Fonin, *Appl. Phys. Lett.,* 2012, **100**, 241606.
57 J. Zhang, Z. Wang, T. Niu, S. Wang, Z. Li and W. Chen, *Sci. Rep.,* 2014, **4**, 4431.

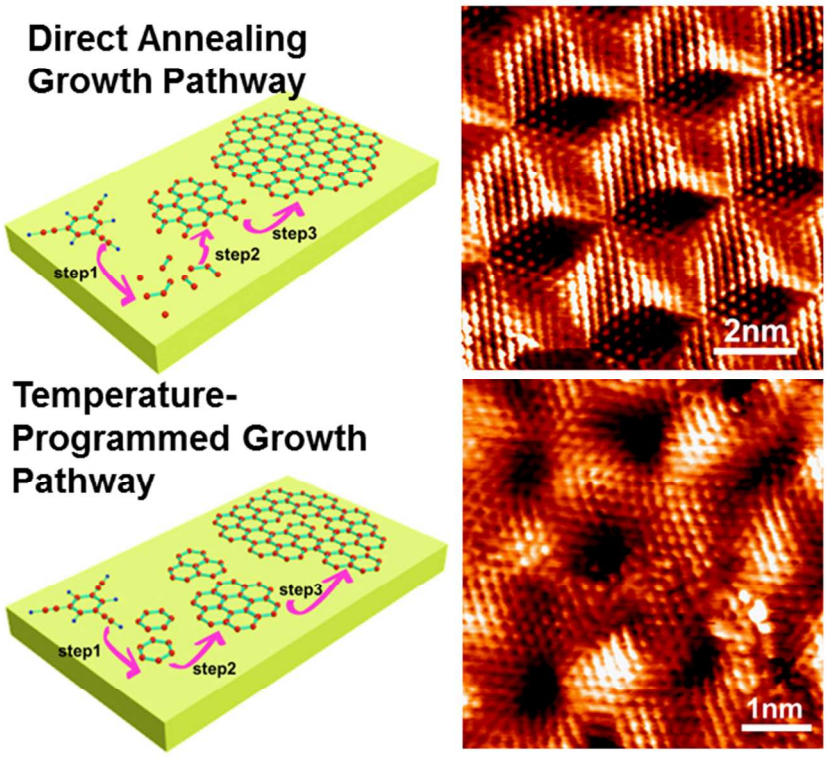

1,3,5-triethynylbenzene (TEB) is selected for the first time as the carbon precursor for graphene synthesis on Rh(111). Considering of the characteristic π-d orbital hybridization between TEB and Rh(111), room-temperature adsorption followed with a temperature-programmed annealing or direct annealing to target growth temperature under the ultrahigh vacuum conditions are designed to be the two synthesis pathways. In the former growth pathway, the benzene ring of the TEB unit is expected to be maintained throughout the whole annealing process, leading to high yielding graphene at relatively low temperature as compared with existing synthesis via gaseous precursors. Interestingly, graphene synthesized via the latter pathway usually possesses less domain boundaries and defects than the former one, probably due to sufficient diffusion and rearrangement of carbon precursors. Briefly, this work should contribute greatly to understanding the growth intermediates and the synthesis of high-quality graphene using large aromatic precursor molecules.
138x113mm (150 x 150 DPI)